Electron scattering by a C_{60} molecule in a projection configuration

1999 J. Phys.: Condens. Matter 11 8617

(http://iopscience.iop.org/0953-8984/11/44/301)

J. Phys.: Condens. Matter **11** (1999) 8617–8631. Printed in the UK PII: S0953-8984(99)05807-5

Electron scattering by a C_{60} molecule in a projection configuration

A Mayer†, P Senet and J-P Vigneron

Laboratoire de Physique du Solide, Facultés Universitaires Notre-Dame de la Paix, Rue de Bruxelles 61, B-5000 Namur, Belgium

E-mail: alexandre.mayer@fundp.ac.be

Received 8 July 1999, in final form 16 September 1999

Abstract. The objective of this paper to discuss the observation of a C_{60} molecule by projection microscopy, in order to highlight the availability of structural information in the sample. In this context, a model for the potential energy relevant to an imaging electron encountering a carbon molecule is developed. The carbon atoms are characterized by static and dynamic polarizabilities to account for the effects of the static extraction bias and the moving imaging electrons. In agreement with previous papers, Fraunhofer and Fresnel diffraction are encountered. The C_{60} molecule turns out to have a strong focusing effect near polarizability resonances. The simulations reveal that, below a given bias, little structural information is available in the potential-energy distribution, due to the large dynamic polarizability of the carbon atoms. Although this information is present for larger bias and appears in the local current density, the resolution of the technique (in its present form) is too limited for the atomic structure of the sample to appear in projected images.

1. Introduction

Projection microscopes make use of the quasi-radial far propagation of field-emitted [1–9] electrons or ions projected out of small tips. Greatly magnified shadows [10] of an object can be obtained, without any lens, on a distant screen by placing the object at short distances from the tip, inside the beam.

In the Fresnel projection microscope (FPM) [11, 12] the electronic source is a tungsten pyramidal nanoprotrusion 2 to 3 nm in height with single-atom sharpness. The object lies on a 3 mm TEM gold grid and the screen is a multiple-channel plate 10 cm distant coupled to a fluorescent screen. The tip-to-sample distance is controlled within one-ångström precision by using technologies developed for the scanning tunnelling microscope. The field-emission voltage, established between the tip holder and the object-supporting grid, is adjusted in the range 50–300 V, a bias which is low enough to avoid all risks of sample destruction. This technique enables typical magnifications of the order of 10^5–10^6 to be achieved and provides projected images of samples with a few nanometres' thickness.

For these small tip-to-sample distances and extraction biases, the wave nature of the imaging electrons cannot be neglected when attempting to understand the image-formation mechanism. Basically, it is the spherical shape of the incoming wave (below critical tip-to-sample distance and sample thickness) that is responsible for the occurrence of Fresnel diffraction images, still highly correlated with direct-space representations of the object.

† Author to whom any correspondence should be addressed.

0953-8984/99/448617+15$30.00

Theoretical support for these electronic projection techniques was given within the Fresnel–Kirchhoff flat-object formalism [13] and the Green's-function formalism [14,15]. Our approach of the problem [16–21] is based on both the transfer-matrix and Green's-function formalisms and enables one to consider the three-dimensional potential-energy distribution between the metallic tip holder and the object-support conducting grid. This allows for simulating the observation of heterogeneous samples by taking account of the strongly varying electric field distribution around the tip and the sample, which is mainly responsible for the position of the virtual projection point [11] and the focusing effect observed with small samples [22].

While our technique enables one to consider general three-dimensional potential-energy distributions, the applications presented in previous papers referred to rather simple situations where the sample is described as a continuous medium. This was appropriate in studying the occurrence of Fraunhofer and Fresnel diffraction [23], sucking-in effects and the observability capacities of the technique [19]. A dipole representation of the tip was considered in reference [21] to show the influence of the tip completeness on contrast. Although the current resolution of projection microscopes (around 0.5 nm) does not reach atomic resolution, it is interesting to take account of the atomic structure of the sample in order to describe efficiently the peculiar conditions encountered in a projection configuration and study the kind of information that is available for observation.

It is the objective of this paper to discuss the observation of a C_{60} molecule by projection microscopy, in order to highlight the availability of structural information in the sample. In this context, a model for the potential energy relevant to the imaging electrons encountering a carbon molecule is developed in section 2. The method used to solve the Schrödinger equation relevant to the imaging electron is summarized in section 3. In section 4, the theory is illustrated by simulated observations of a C_{60} molecule by projection microscopy. Fraunhofer and Fresnel diffraction are encountered. The focusing effect of the molecule is demonstrated. The simulations reveal that, below a given bias, little structural information is available in the potential-energy distribution, due to the large dynamic polarizability of the carbon atoms. Although this information is present for larger bias, the resolution of the technique (in its present form) is too limited for the atomic structure of the sample to be observed.

2. Potential energy for an imaging electron encountering a carbon molecule

2.1. Basic formulation

Let us consider a given electron that escapes from the tip holder by a field-emission process. Due to the low emission current (less than 1 nA for a single nanotip), it is reasonable to consider these electrons individually (the exchange and correlation effects due to the other electrons in the metallic tip holder being empirically described by suitable values of the Fermi energy E_F and work function W).

Before reaching the imaging screen, this electron encounters a carbon molecule with N electrons. By assuming the carbon nuclei to keep a fixed position, the problem to solve is that of the wave function of $N+1$ electrons. Within the density functional theory (DFT) [24], these electrons are described by $N+1$ orbitals Ψ_i that obey the following coupled equations:

$$\left(-\frac{\hbar^2}{2m}\nabla^2 + V^{eff}\right)\Psi_i(\boldsymbol{r}) = E_i\Psi_i(\boldsymbol{r}). \tag{1}$$

The subscript 0 will refer conventionally to the imaging electron, while the N others refer to the electrons belonging to the carbon molecule.

The effective potential V^{eff} in equation (1) results from $V^{eff} = V_{ext} + V_{ion} + V_{elec}$. The first term V_{ext} is the potential-energy distribution that results from the extraction bias. This term also contains the interaction with the other electrons in the metallic tip holder, which, as stated earlier, is determined by empirical values of E_F and W. V_{ext} can be computed by relaxation methods (see reference [17]) or by a dipole model (see reference [16]) according to whether the tip is described as a continuous medium or an atomic structure.

The interaction with the carbon nuclei is described by the second term

$$V_{ion}(\boldsymbol{r}) = -\frac{e^2}{4\pi\epsilon_0}\sum_j \frac{Z_j}{|\boldsymbol{r}-\boldsymbol{R}_j|} \tag{2}$$

where $Z_j e$ and $\boldsymbol{R}_j$ are respectively the charge and position of each nucleus.

The last term V_{elec} stands for all effects due to electronic interactions (i.e. repulsion, exchange and correlation). It will be evaluated in the next subsection.

2.2. Reduction of the molecular electronic structure to an electron density

There are $N + 1$ coupled equations like equation (1) to solve self-consistently. However, for the purpose of simulating projected images, we are only interested in determining the state Ψ_0 associated with the imaging electron. The problem can therefore be simplified by reducing the description of the N other electrons to a molecular electron density

$$\rho^{molec}(\boldsymbol{r}) = \sum_{j=1}^{N} |\Psi_j(\boldsymbol{r})|^2$$

described by a model. The Hartree and exchange terms relevant to the imaging electron 0 can be estimated from this model electronic density $\rho^{molec}(\boldsymbol{r})$. Correlation will be evaluated by a perturbational approach.

If v_{HX} is the potential associated with the Coulombic and exchange interactions between the imaging electron 0 and the molecular density ρ^{molec}, the potential energy corresponding to the Hartree, exchange and correlation terms is given in a second-order approximation by [25]

$$V_{elec}(\boldsymbol{r}) = \int \rho_0^{molec}(\boldsymbol{r}')v_{HX}(\boldsymbol{r},\boldsymbol{r}')\,\mathrm{d}\boldsymbol{r}' + \frac{1}{2}\int \delta\rho^{molec}(\boldsymbol{r}')\,v_{HX}(\boldsymbol{r},\boldsymbol{r}')\,\mathrm{d}\boldsymbol{r}' \tag{3}$$

where $\delta\rho^{molec}$ is the perturbation of the equilibrium configuration ρ_0^{molec} due to the imaging electron 0. The second term in equation (3) includes correlation effects.

Ignoring non-local exchange effects, we can model the potential v_{HX} as

$$v_{HX}(\boldsymbol{r},\boldsymbol{r}') = \frac{1}{4\pi\epsilon_0}\frac{e^2}{|\boldsymbol{r}-\boldsymbol{r}'|} + \frac{4}{3}C_X(\rho_0^{molec}(\boldsymbol{r}))^{-2/3}\delta(\boldsymbol{r}-\boldsymbol{r}') \tag{4}$$

with

$$C_X = -\frac{3}{4}\left(\frac{e^2}{4\pi\epsilon_0}\right)\left(\frac{3}{\pi}\right)^{1/3}.$$

The potential energy V_{elec} becomes, according to equation (3),

$$V_{elec}(\boldsymbol{r}) = V_1(\boldsymbol{r}) + V_2(\boldsymbol{r}) \tag{5}$$

with

$$V_1(\boldsymbol{r}) = \frac{e^2}{4\pi\epsilon_0}\int \frac{\rho_0^{molec}(\boldsymbol{r}')}{|\boldsymbol{r}-\boldsymbol{r}'|}\,\mathrm{d}\boldsymbol{r}' + \frac{4}{3}C_X\left[\rho_0^{molec}(\boldsymbol{r})\right]^{1/3} \tag{6}$$

$$V_2(\boldsymbol{r}) = \frac{1}{2}\frac{e^2}{4\pi\epsilon_0}\int \frac{\delta\rho^{molec}(\boldsymbol{r}')}{|\boldsymbol{r}-\boldsymbol{r}'|}\,\mathrm{d}\boldsymbol{r}' + \frac{2}{3}C_X\left[\rho_0^{molec}(\boldsymbol{r})\right]^{-2/3}\,\delta\rho^{molec}(\boldsymbol{r}). \tag{7}$$

V_1 is the sum of the Hartree electronic repulsion term and of the local density approximation (LDA) exchange potential. V_2 is a second-order correction taking account of correlation effects between the imaging electron and the N electrons of the molecular target.

2.3. Description of the molecular electron density by Gaussian distributions

In a crude approximation, we model the valence electrons of each carbon atom by Gaussian distributions that can move rigidly around the nuclei positions. The core electrons are frozen, so their only effect is to reduce the effective value of the nuclear charge Z_j from 6 to 4. The parameters of the Gaussian distributions are fixed according to results [26] relevant to the quantum harmonic potential in a constant electric field E. Since the solutions of this problem are moved by $\Delta x = eE/(m\omega_j^2)$ and the polarization of an atom j is given by $p_j = \alpha_j E = (Z_j e)\,\Delta x$, we can relate the characteristic pulsation ω_j of a given atom j to its polarizability α_j by

$$\omega_j = e\sqrt{\frac{Z_j}{m\alpha_j}}. \tag{8}$$

Because the solutions of this problem are all proportional to $\exp(-[m\omega_j/(2\bar{h})]r^2)$, the electron density corresponding to an atom j will be modelled by

$$\rho_j^{atom}(\boldsymbol{r}) = \frac{Z_j}{\pi^{3/2}\bar{R}_j^3}\mathrm{e}^{-|\boldsymbol{r}-\boldsymbol{r}_j|^2/\bar{R}_j^2} \tag{9}$$

where the radius $\bar{R}_j$ is given by

$$\bar{R}_j = \sqrt{\frac{\bar{h}}{m\omega_j}} = \sqrt{\frac{\bar{h}}{e}}\left(\frac{\alpha_j}{mZ_j}\right)^{1/4}.$$

The position of the centre $\boldsymbol{r}_j$ of the electron density $\rho_j^{atom}(\boldsymbol{r})$ is obtained by computing in a first step the polarization $\boldsymbol{p}_j$ of each atom j and by applying in a second step the relation $\boldsymbol{p}_j = Z_j e(\boldsymbol{R}_j - \boldsymbol{r}_j)$. The computation of the dipoles $\boldsymbol{p}_j$ is done by solving the linear system of equations $\boldsymbol{p}_j = \alpha_j \boldsymbol{E}_j$, where $\boldsymbol{E}_j$ is the total electric field exerted on the dipole $\boldsymbol{p}_j$ by the other dipoles and the relevant external agents (i.e. the extraction bias and the imaging electron). Details are given in appendix B of reference [16].

The molecular electron density ρ^{molec} is finally given by

$$\rho^{molec}(\boldsymbol{r}) = \sum_j \rho_j^{atom}(\boldsymbol{r}). \tag{10}$$

The integrals encountered in the computation of the electronic repulsion terms are evaluated according to

$$\frac{e^2}{4\pi\epsilon_0}\int \frac{\rho^{molec}(\boldsymbol{r}')}{|\boldsymbol{r}-\boldsymbol{r}'|}\,\mathrm{d}\boldsymbol{r}' = \frac{e^2}{4\pi\epsilon_0}\sum_j Z_j \frac{\mathrm{erf}(|\boldsymbol{r}-\boldsymbol{r}_j|/\bar{R}_j)}{|\boldsymbol{r}-\boldsymbol{r}_j|}. \tag{11}$$

2.4. Static and dynamic polarizabilities

The values of polarizability to consider for the static electric bias and the moving imaging electron are not the same. When computing the potential-energy distribution due to the electric bias, the static polarizability α_{stat} of the carbon atoms has to be considered. When computing

the contribution due to the imaging electron, the dynamic polarizability $\alpha_{dyn}(\omega)$ of the carbon atoms should be considered. E and ω are related by $E = \hbar\omega$.

According to reference [27], the dynamic polarizability of the carbon atoms in the C_{60} molecule can be evaluated from

$$\alpha_{dyn}(\omega) = \frac{\alpha_{stat}}{1 - \omega^2/\omega_c^2} \tag{12}$$

where the volumic static polarizability $\alpha_{stat}/(4\pi\epsilon_0)$ and the characteristic energy $\hbar\omega_c$ take respectively the values 1.100 Å^3 and 18.15 eV.

2.5. The final expression

To summarize this section, the effective potential energy V_{eff} relevant to the imaging electron is computed in two steps. In the first step, one has to compute the first-order contribution $V_1(\boldsymbol{r})$ at a given point $\boldsymbol{r}$ that results from the extraction bias and from exchange effects only. The atoms are characterized by the static polarizability α_{stat} that is associated with the radius $\bar{R}_j$. The external potential energy V_{ext} and the associated electric field take account of the extraction bias and the emission tip. V_{ext} can be computed by the methods of reference [17] if the tip is described as a continuous medium. The techniques of appendix B in reference [16] are then used to compute the dipoles $\boldsymbol{p}_j$ associated with each carbon atom. These values enable the electronic displacements $\Delta\boldsymbol{r}_j$ to be defined by the relation $\boldsymbol{p}_j = -Z_j e\,\Delta\boldsymbol{r}_j$. The positions $\boldsymbol{r}_j$ of the electron densities in the equilibrium configuration ρ_0 are calculated according to $\boldsymbol{r}_j = \boldsymbol{R}_j + \Delta\boldsymbol{r}_j$.

In the second step, one has to compute the second-order correction $V_2(\boldsymbol{r})$ due to correlation effects (i.e. the polarization of the molecule induced by the imaging electron at $\boldsymbol{r}$). The atoms are characterized by the dynamic polarizability $\alpha_{dyn}(E/\hbar)$ that is associated with the radius $\bar{R}'_j$. The dipoles $\boldsymbol{p}'_j$ associated with each carbon atom are computed in the same way as previously, by considering the electric field due to the imaging electron at $\boldsymbol{r}$ only. These values enable the new electronic displacements $\Delta\boldsymbol{r}'_j$ to be defined by the relation $\boldsymbol{p}'_j = -Z_j e\,\Delta\boldsymbol{r}'_j$. The positions $\boldsymbol{r}'_j$ of the electron densities in the modified configuration $\rho_0 + \delta\rho$ are calculated according to $\boldsymbol{r}'_j = \boldsymbol{R}_j + \Delta\boldsymbol{r}_j + \Delta\boldsymbol{r}'_j$.

These two contributions enable V^{eff} to be finally computed from

$$\begin{aligned} V^{eff}(\boldsymbol{r}) = V_{ext}(\boldsymbol{r}) &- \frac{e^2}{4\pi\epsilon_0}\sum_j \frac{Z_j}{|\boldsymbol{r} - \boldsymbol{R}_j|} \\ &+ \frac{1}{2}\frac{e^2}{4\pi\epsilon_0}\sum_j Z_j\left[\frac{\operatorname{erf}(|\boldsymbol{r} - \boldsymbol{r}_j|/\bar{R}_j)}{|\boldsymbol{r} - \boldsymbol{r}_j|} + \frac{\operatorname{erf}(|\boldsymbol{r} - \boldsymbol{r}'_j|/\bar{R}'_j)}{|\boldsymbol{r} - \boldsymbol{r}'_j|}\right] \\ &+ \frac{2}{3}C_X\left(\sum_j \frac{Z_j}{\pi^{3/2}\bar{R}_j^3}\mathrm{e}^{-|\boldsymbol{r}-\boldsymbol{r}_j|^2/\bar{R}_j^2}\right)^{1/3} \\ &\times\left[1 + \left(\sum_j \frac{Z_j}{\bar{R}_j'^3}\mathrm{e}^{-|\boldsymbol{r}-\boldsymbol{r}'_j|^2/\bar{R}_j'^2}\right)\Big/\left(\sum_j \frac{Z_j}{\bar{R}_j^3}\mathrm{e}^{-|\boldsymbol{r}-\boldsymbol{r}_j|^2/\bar{R}_j^2}\right)\right]. \end{aligned} \tag{13}$$

The potential energy at the atomic positions is truncated at the value $-E_{ea} - \hbar\omega_{stat}/2$, where $E_{ea} = 2.74$ eV is the electron affinity of the C_{60} molecule [28] and ω_{stat} the pulsation associated by equation (8) with the static polarizability α_{stat} of the carbon atoms. This value is the depth of the harmonic potential whose fundamental state is at the level the incident electron would occupy in the case of absorption. To avoid the last term of equation (13) diverging, the second-order correction for exchange effects should only be considered when $\bar{R}'_j < \bar{R}_j$.

3. Electronic scattering by transfer matrices and Green's functions

In the present model, the metallic tip holder is described by using a simple Sommerfeld picture, characterized with empirical values of W (the work function) and E_F (the Fermi energy). The tip holder is limited by the plane $z = 0$. This metallic region $z \leqslant 0$, with constant potential energy, is referred to as 'region I'. The conducting grid is in the plane $z = D$. The region $z \geqslant D$, where the potential energy is set conventionally to the constant value 0, is referred to as 'region III'. We refer to the intermediate region $0 \leqslant z \leqslant D$, that contains the emission tip and the sample, as 'region II'.

In order to take advantage of situations where the z-axis corresponds to a n-fold symmetry, the scattering problem was formulated in cylindrical coordinates [16–19], by using the polar coordinates ϕ (azimuthal angle) and ρ (radial distance to the axis) in the plane normal to the z-axis. Following reference [29], the scattering electrons are assumed to remain localized inside a cylinder of radius R in the regions I and II.

Since the potential energy is constant for $z \leqslant 0$ and $z = D$, the wave function associated with the imaging electron can be expanded in these two regions in well-defined basic states. The basic states relevant to region I and to the plane $z = D$ are written respectively as $\Psi_j^{I,\pm}$ and $\Psi_j^{D,\pm}$, where the + and − subscripts refer to the propagation direction relative to the z-axis.

Within the transfer-matrix methodology, the scattering problem can be solved in the intermediate region II [16–18]. This first part of the procedure provides the solutions corresponding to single incident basic states $\Psi_j^{I,+}$ in region I. These solutions are expanded in region I and for $z = D$ according to

$$\Psi_j^+ \overset{z\leqslant 0}{=} \Psi_j^{I,+} + \sum_i t_{i,j}^{-+} \Psi_i^{I,-} \overset{z=D}{=} \sum_i t_{i,j}^{++} \Psi_i^{III,+} \tag{14}$$

where the coefficients of the expansion are stored in the transfer matrices $\mathbf{t}^{++}$ and $\mathbf{t}^{-+}$.

Within the Green's-function formalism and with the Kirchhoff assumption [30] that we can use the expression obtained by the transfer-matrix method for the wave function and its derivatives in the plane $z = D$, the solutions Ψ_j^+ can be propagated from this plane $z = D$ to the distant imaging screen by an expression of the form [19]

$$\Psi_j^+(r, \theta, \phi) \overset{r\gg 0}{=} \frac{\mathrm{e}^{\mathrm{i}k_E r}}{r} \sum_i t_{i,j}^{++} \sigma(\theta, \phi, i, E) \tag{15}$$

with

$$k_E = \sqrt{\frac{2mE}{\hbar^2}}$$

and $\sigma(\theta, \phi, i, E)$ analytic coefficients.

The total current density on the conducting grid results from the contribution of all solutions Ψ_j^+. These contributions are weighted by the density of states associated with each state $\Psi_j^{I,+}$ in the metallic region I.

The time and storage space required by a transfer-matrix treatment of the local scattering are significantly reduced compared to those encountered with a Green's-function [14, 15] or finite-element [29] formulation. In the present transfer-matrix approach, these requirements are typically proportional to nb^3 and $DE^{1/2}nb^3$, where nb is the number of basic states to consider simultaneously. This number nb can be reduced systematically by consideration of group theory (see reference [18]). The numerical instabilities encountered in the derivation of the solutions given in equation (14) can be controlled by the techniques given in references [20,31]. A generalization of this formalism to non-square matrices is presented in reference [18].

4. Simulated observation of a C_{60} molecule by projection microscopy

The technique presented in the previous section has been applied to simulate field emission from nanotips [21] and the observation of carbon fibres by projection microscopy [23]. The present application aims at simulating the observation of a C_{60} molecule by the same technique, by focusing on the availability of structural information in the potential-energy distribution encountered by the imaging electron. The occurrence of Fraunhofer and Fresnel diffraction as well as the focusing effect of the C_{60} molecule are illustrated.

To characterize the metallic support of the tip, we considered a Fermi energy E_F of 19.1 eV and a work function W of 4.5 eV (values for tungsten). The emission tip is represented by a cone with a height and base diameter of 1 nm. The atoms of the C_{60} molecule are modelled according to section 2. The C_{60} is assumed to lie on a pentagonal ring, so z is a fivefold-symmetry axis. According to group theory [18], there are five independent sets of basic states that can be treated separately.

For the first simulation, the distance D between the tip holder and the conducting grid is 3.5 nm. The extraction bias V is 10 V. The electron energy E (5.5 eV) is smaller than the characteristic energy (18.15 eV) of the atoms in the C_{60} molecule so the static and dynamic polarizabilities are of similar magnitude ($\alpha_{dyn} \simeq 1.1\alpha_{stat}$). The potential-energy distribution in region II is illustrated in figure 1 by a vertical section in the xz-plane. The atoms of the C_{60} molecule do not appear individually in the potential-energy distribution and the molecule has an attractive effect on the incident electron. This behaviour can be explained by the large values of the polarizability that are responsible for the electrons of the C_{60} molecule moving

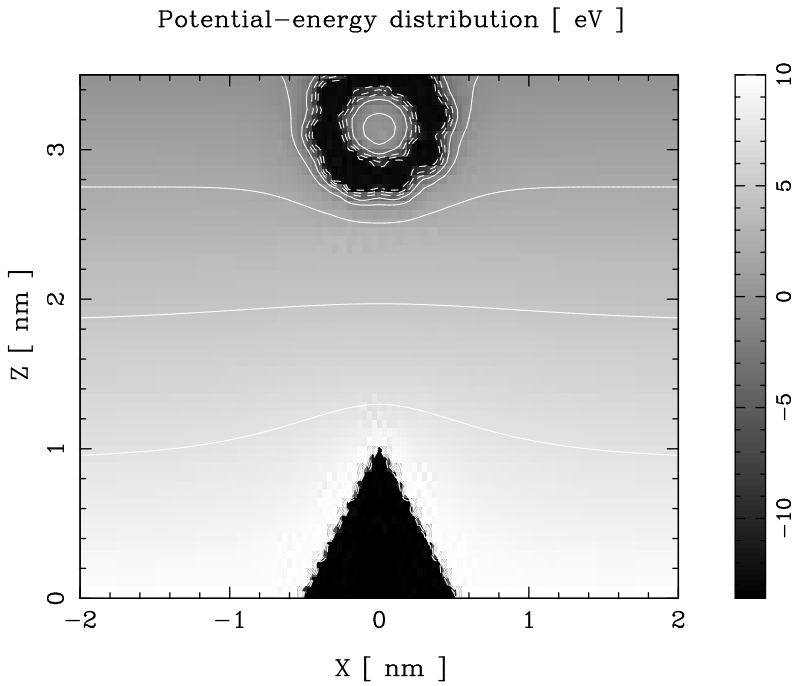

Figure 1. The potential-energy distribution in the xz-plane. A C_{60} molecule is observed in a virtual projection microscope. The extraction bias and the distance between the tip holder and the conducting grid are respectively 10 V and 3.5 nm.

away from the incident electron, with the result that it is attracted by the positive nuclei that remain closer. The total current density on the conducting grid and on the screen 10 cm distant are illustrated in figure 2. The local current density highlights the strong focusing effect of the C_{60} molecule.

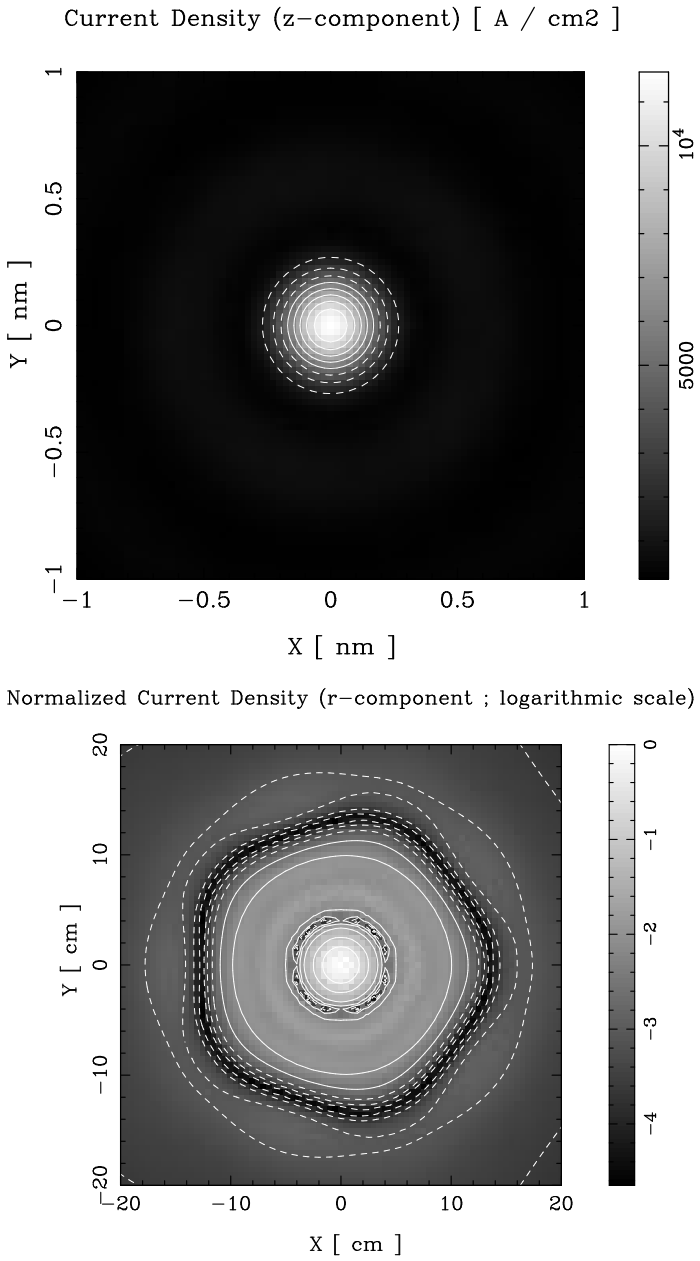

Figure 2. The current density (in A cm^{-2}) on the conducting grid (top) and (on a logarithmic scale) on the screen 10 cm distant (bottom). A C_{60} molecule is observed in a virtual projection microscope. The extraction bias and the distance between the tip holder and the conducting grid are respectively 10 V and 3.5 nm.

This effect is better illustrated in figure 3, where the current densities obtained with and without the molecule are compared. The long-range current density, represented on a logarithmic scale, is a Fraunhofer figure. The fivefold symmetry is clearly visible. The occurrence of Fraunhofer diffraction is expected since the resolution limit due to diffraction ($\Delta_d = \frac{1}{2}\sqrt{\lambda d} = 0.53$ nm) is larger than the molecule radius.

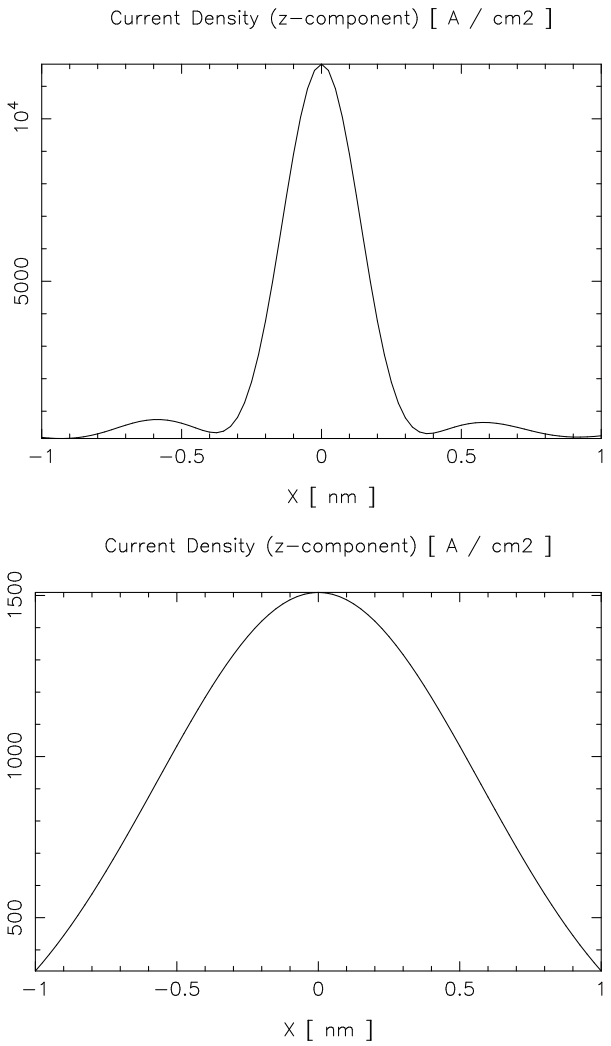

Figure 3. The current density (in A cm^{-2}) on the conducting grid with (top) and without (bottom) the C_{60} molecule. The extraction bias and the distance between the tip holder and the conducting grid are respectively 10 V and 3.5 nm.

For the second simulation, an extraction bias of 25 V and a metal–grid distance of 3 nm are considered. The electron energy E (20.5 eV) is close to the characteristic energy (18.15 eV) of the atoms in the C_{60} molecule, so the dynamic polarizability is enlarged ($\alpha_{dyn} \simeq -4.4\alpha_{stat}$). The corresponding potential-energy distribution in region II is illustrated in figure 4. The potential wells surrounding the carbon atoms are enlarged. This behaviour is due to the dynamic polarizability being larger than in the previous simulation. The total current density on the

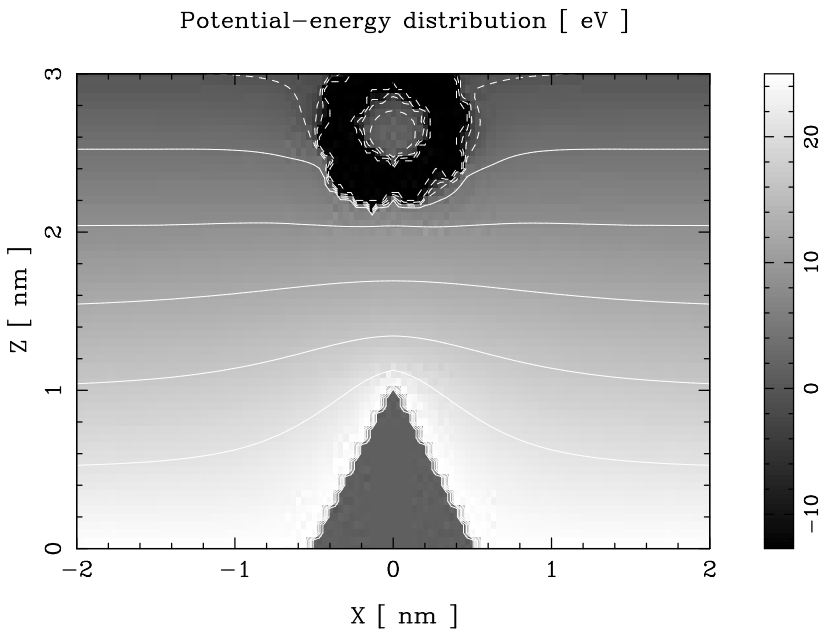

Figure 4. The potential-energy distribution in the xz-plane. A C_{60} molecule is observed in a virtual projection microscope. The extraction bias and the distance between the tip holder and the conducting grid are respectively 25 V and 3 nm.

conducting grid and on the screen 10 cm distant are illustrated in figure 5. The local current density reveals a stronger focusing effect that is responsible for the imaging electrons travelling exclusively through the envelope of the molecule. The long-range current density is a Fresnel figure. This is expected since the resolution limit due to diffraction ($\Delta_d = \frac{1}{2}\sqrt{\lambda d} = 0.34$ nm) is approximately the molecule radius. The figure is similar to that for the local current density and reveals the global spherical shape of the molecule by enforcing its edge.

In the last simulation, an extraction bias of 40 V and a metal–grid distance of 4 nm are considered. The electron energy E (35.5 eV) is beyond the polarization resonance and the dynamic polarizability is significantly reduced ($\alpha_{dyn} \simeq -0.37\alpha_{stat}$). The potential-energy distribution in region II is illustrated in figure 6. The figure reveals a potential-energy distribution that exhibits strongly localized variations at the atomic positions. This behaviour is due to the reduced dynamic polarizability. The total current density on the conducting grid and on the screen 10 cm distant are illustrated in figure 7. The local current density shows the electronic beam that results from the field-emission process. The focusing effect is strongly reduced due to the smaller dynamic polarizability of the carbon atoms. The sharper variations in the central part of the figure are the result of the wavelength of the incident electron being reduced. They are related to the atomic structure of the C_{60} molecule. The long-range current density is a Fresnel figure ($\Delta_d = 0.37$ nm), where again only the global spherical shape of the molecule is visible, despite the fact that the atomic structure appears in the potential-energy distribution and in the current density on the conducting grid. The lack of information on the atomic structure of the molecule in the projected image is due to the limited resolution of the technique. The enforcement of the edge of the figure is less pronounced than in the previous simulation due to the reduction of the number of electrons that travel through the envelope of the molecule.

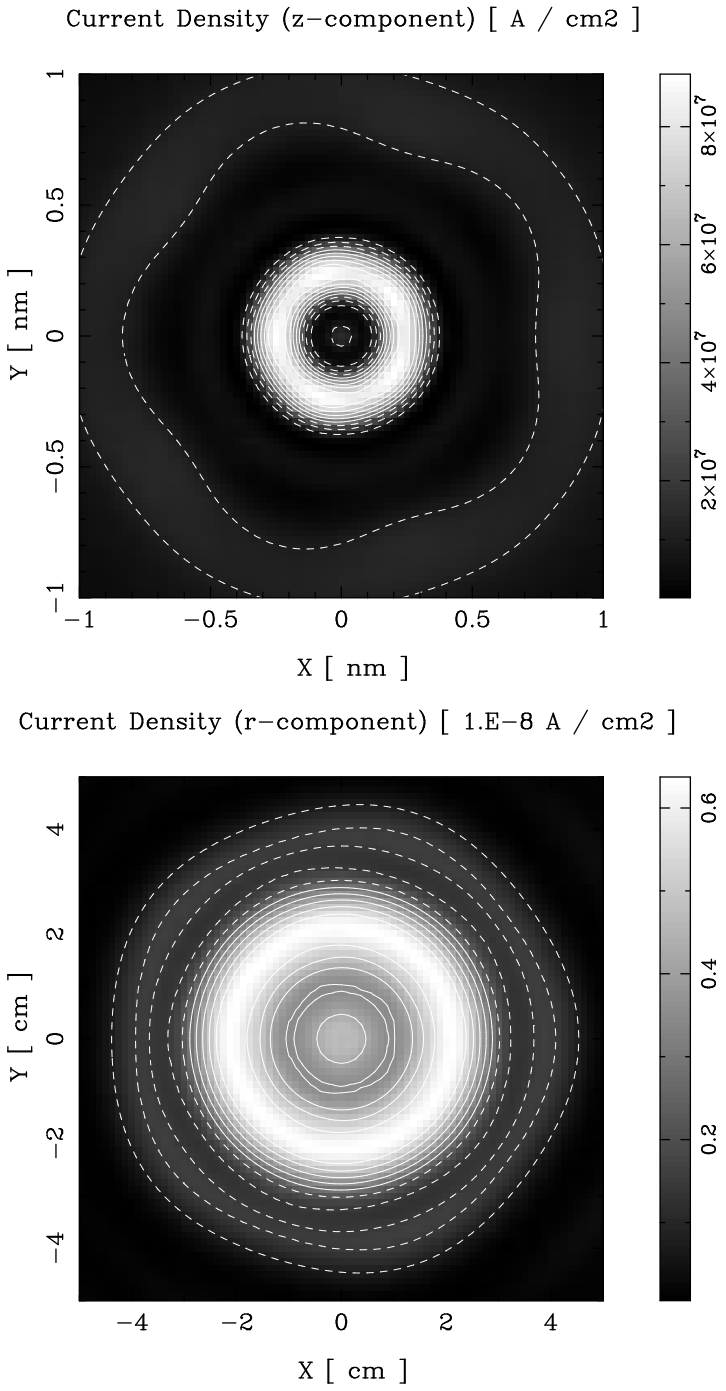

Figure 5. The current density (in A cm^{-2}) on the conducting grid (top) and on the screen 10 cm distant (bottom). A C_{60} molecule is observed in a virtual projection microscope. The extraction bias and the distance between the tip holder and the conducting grid are respectively 25 V and 3 nm.

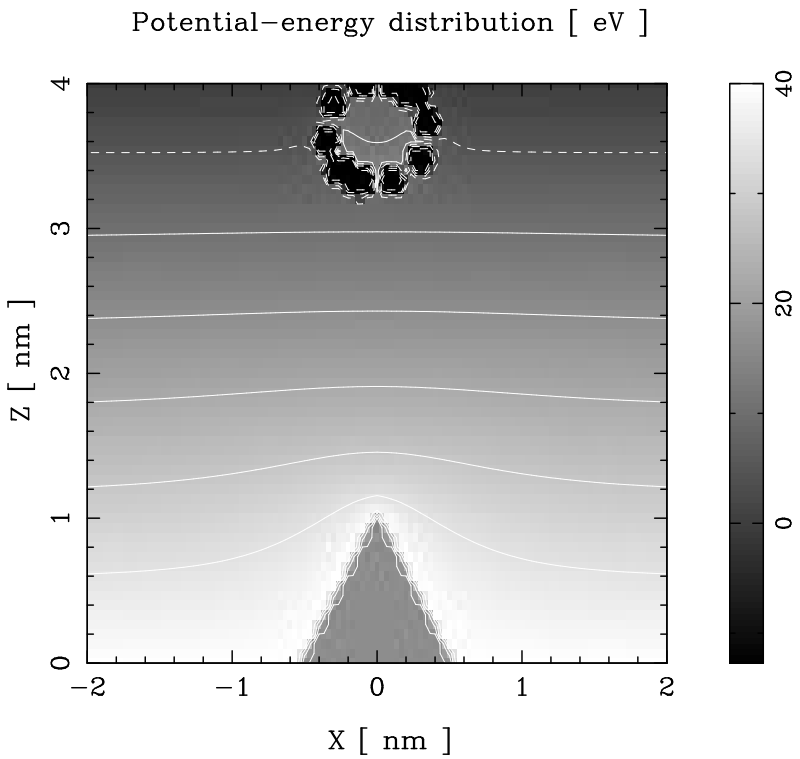

Figure 6. The potential-energy distribution in the xz-plane. A C_{60} molecule is observed in a virtual projection microscope. The extraction bias and the distance between the tip holder and the conducting grid are respectively 40 V and 4 nm.

Comparison between the results obtained when correlation is considered and when it is not proves the necessity of taking this effect into consideration, especially when the energy of the incident electron is close to the plasmon energy $\hbar\omega_c$ of the target molecule (like in the first two simulations). The polarization of the molecule induced by the imaging electron is responsible for the focusing effect and the potential wells associated with each carbon atom being enlarged, thus reducing corrugations related to the atomic structure. The result on a distant screen is mainly a higher confinement of the beam in the central part of the figure. The effects of correlation tend however to disappear as the energy of the incident electron increases. The last simulation (with a 40 V bias) is representative of the results obtained when correlation is negligible.

5. Conclusions

In order to discuss the observation of a C_{60} molecule by projection microscopy, a model for the potential energy relevant to the imaging electrons encountering a carbon molecule had to be developed. Despite some crude approximations, this model takes account of the polarization of the carbon atoms due to the static electric bias and the moving imaging electron. The dynamic aspect of the problem is treated by a second-order correction for correlation effects and the consideration of static and dynamic polarizabilities. Exchange effects are considered in the LDA approximation. The description of the electronic structure of the molecule can be

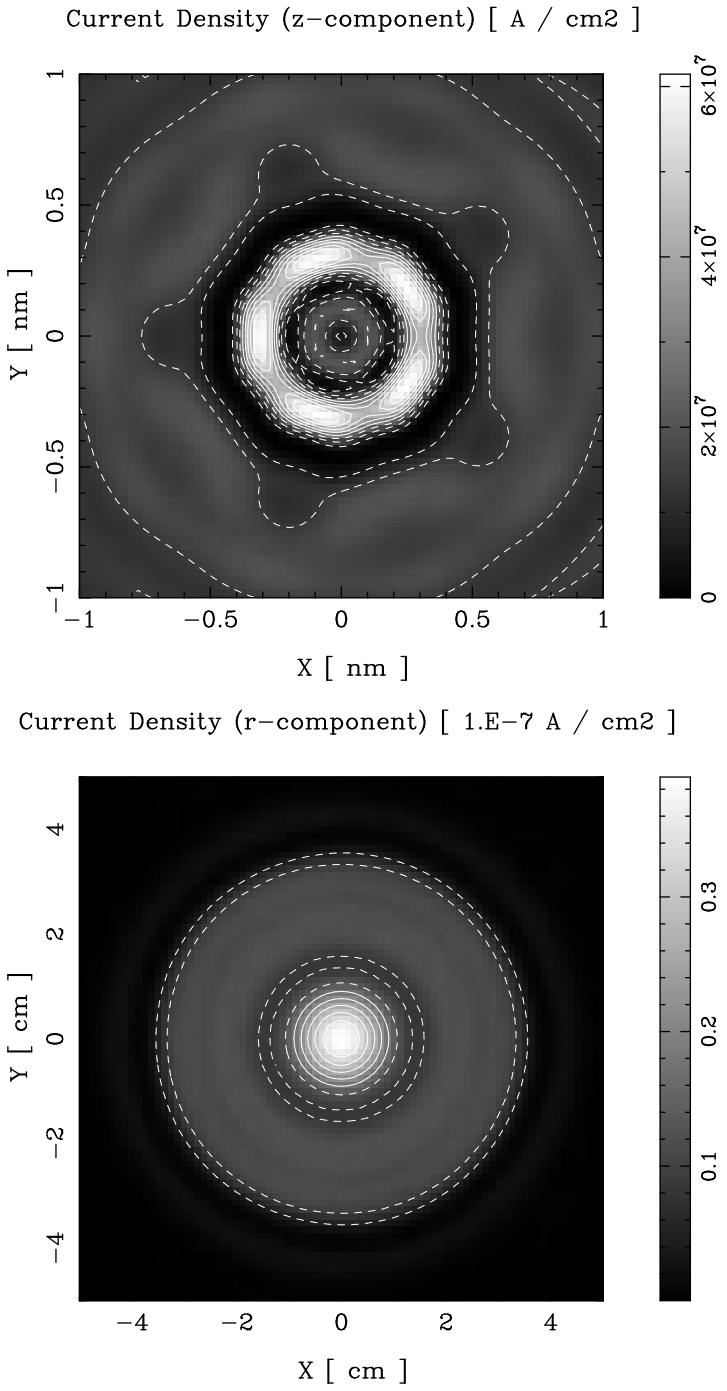

Figure 7. The current density (in A cm^{-2}) on the conducting grid (top) and on the screen 10 cm distant (bottom). A C_{60} molecule is observed in a virtual projection microscope. The extraction bias and the distance between the tip holder and the conducting grid are respectively 40 V and 4 nm.

improved if atomic orbitals (instead of Gaussian distributions) are considered for computing the equilibrium and modified molecular configurations. The potential-energy distribution can still be improved by a self-consistent-field (SCF) computation, provided that the long-range correlation (image interaction) is appropriately represented.

In agreement with previous papers, Fraunhofer or Fresnel diffraction is encountered according to whether the resolution limit due to diffraction $\Delta_d = \frac{1}{2}\sqrt{\lambda d}$ is larger or smaller than one half of the sample thickness. In the light of this paper, it turns out that the decrease of the dynamic polarizability of the carbon atoms with the extraction bias (beyond polarization resonances) is responsible for the focusing effect of the C_{60} molecule and the extension of the potential wells representing each carbon atom being both reduced. As a consequence of these reductions, the potential-energy distribution encountered by the imaging electron has intrinsically more information on the atomic structure of the sample for higher values of the extraction bias. These values (50–300 V) are typically those operated in the Fresnel projection microscope. The simulations reveal that this structural information is present in the local current density. However, it does not appear in projected images, due to the limited resolution of the technique in its present form.

Acknowledgments

AM and PS were supported by the Belgian National Fund for Scientific Research (FNRS). The authors acknowledge the national programme on the Interuniversity Research Project (PAI) and the use of the Namur Scientific Computing Facility, a common project of the FNRS, IBM-Belgium and the FUNDP. The authors are grateful to Ph Lambin and M Devel for useful discussions.

References

[1] Fowler R H and Nordheim L 1928 *Proc. R. Soc.* A **119** 173
[2] Good R H and Müller E 1956 *Handbuch der Physik* vol 21 (Berlin: Springer) p 176
[3] Burgess R E, Kroemer H and Houston J M 1953 *Phys. Rev.* **90** 515
[4] Young D R 1959 *Phys. Rev.* **113** 110
[5] Stratton R 1964 *Phys. Rev.* A **135** 794
[6] Swanson L W and Crouser L C 1967 *Phys. Rev.* **163** 622
[7] He J, Cutler P H, Miskovsky N M, Feuchtwang T E, Sullivan T E and Chung M 1991 *Surf. Sci.* **246** 348
[8] Cutler P H, He J, Miskovsky N M, Sullivan T E and Weiss B 1992 *J. Vac. Sci. Technol.* B **11** 387
[9] Jensen K L and Zaidman E G 1993 *J. Vac. Sci. Technol.* B **12** 776
[10] Melmed A J 1968 *Appl. Phys. Lett.* **12** 100
[11] Binh V T, Semet V and Garcia N 1995 *Ultramicroscopy* **58** 307
[12] Binh V T and Semet V 1998 *Ultramicroscopy* **73** 107
[13] Binh V T, Semet V, Garcia N and Bitar L 1996 *Optics at the Nanometre Scale* ed M Nieto-Vesperinas and N Garcia (Dordrecht: Kluwer) p 277
[14] Kreuzer H J, Nakamura K, Wierzbicki A, Fink H-W and Schmid H 1992 *Ultramicroscopy* **45** 381
[15] Mayer A, Castiaux A and Vigneron J-P 1998 *Comput. Phys. Commun.* **109** 81
[16] Mayer A and Vigneron J-P 1997 *Phys. Rev.* B **56** 12 599
[17] Mayer A and Vigneron J-P 1998 *J. Phys.: Condens. Matter* **10** 869
[18] Mayer A and Vigneron J-P 1999 *Phys. Rev.* E submitted
[19] Mayer A and Vigneron J-P 1999 *Phys. Rev.* B **60**
[20] Mayer A and Vigneron J-P 1999 *Phys. Rev.* E **59** 4687
[21] Mayer A and Vigneron J-P 1999 *J. Vac. Sci. Technol.* B **17** 506
[22] Binh V T and Semet V 1998 *Ultramicroscopy* **73** 107
[23] Mayer A and Vigneron J-P 1999 *Ultramicroscopy* **79** 35
[24] Maghan G D and Subbaswamy K R 1990 *Local Density Theory of Polarizability* (New York: Plenum)
[25] Senet P 1996 *J. Chem. Phys.* **105** 6471

[26] Cohen-Tannoudji C, Diu B and Laloë F 1973 *Mécanique Quantique* (Paris: Hermann)
[27] Gravil P A, Devel M, Lambin P, Bouju X, Girard C and Lucas A A 1996 *Phys. Rev.* B **53** 1622
[28] Yang S H, Pettiette C L, Conceico J, Chesnovsky O and Smalley R E 1987 *Chem. Phys. Lett.* **139** 233
[29] Laloyaux T, Derycke I, Vigneron J P, Lambin P and Lucas A A 1993 *Phys. Rev.* B **47** 7508
[30] Jackson J D 1962 *Classical Electrodynamics* 2nd edn (New York: Wiley) p 427
[31] Pendry J B 1974 *Low Energy Electron Diffraction* (London: Academic)